

## Design of the Tolerance Ring in the Actuator Arm of a Hard Disk Drive Using Finite Element Analysis

Somkid Suthaweesub<sup>1</sup> and Arbtip Dheeravongkit<sup>2</sup>

<sup>1</sup>King Mongkut's University of Technology Thonburi, Thailand, [sutsomkid@yahoo.com](mailto:sutsomkid@yahoo.com)

<sup>2</sup>King Mongkut's University of Technology Thonburi, Thailand, [arbtip@fibo.kmutt.ac.th](mailto:arbtip@fibo.kmutt.ac.th)

### ABSTRACT

This paper presents conceptual designs of the hard disk drive's tolerance ring in order to reduce the installation force during the assembly process of the actuator arm and to decrease the total deformation of the tolerance ring, while maintaining the natural frequency within the specification range. In this research, the finite element analysis is employed to compare and analyze the installation forces, total deformations of tolerance ring, and natural frequencies of Actuator Pivot Flex Assembly (APFA). Around its cylindrical body, the tolerance ring consists of several waves, which provide stiffness for the APFA assembly to resist the axial rocking motion of the actuator arm. The idea is to decrease the contact surface area between the waves and the e-block by smoothing the contacting surface of the waves along the installation direction, while keeping enough friction to resist the axial rocking motion. This research examines five designs of tolerance ring's wave, including the vertical and horizontal curve designs, the symmetric and asymmetric wave designs, and the alternating flat-curve design. The finite element analysis results show that the concept of the horizontal curve design is better than the vertical curve design, since it effectively decreases both the installation force and the total deformation of the tolerance ring, while the natural frequency of the pivot butterfly mode remains within the specification range. However, the alternating flat-curve design can keep the installation force and the natural frequency closer to the mid values of the specification range than other designs.

**Keywords:** hard disk drive, finite element analysis, tolerance ring, mechanical vibration, natural frequency.

DOI: 10.3722/cadaps.2011.xxx-yyy

### 1 INTRODUCTION

Hard Disk Drive (HDD) is a digital magnetic data storage device which consists of Head Stack Assembly (HSA), Actuator Pivot Flex Assembly (APFA), Head Gimbal Assembly (HGA) and other components. During the read and write process of HDD, the HGAs are controlled to move back and forth on the spinning disks. The actuator is controlled to move very fast, which may cause unwanted resonance and damage to the operation of the drive.

Generally in HDD, the actuator arm is fixed to the pivot bearing with a tolerance ring as shown in Fig. 1. The tolerance rings are made of stainless steel and provide the stiffness for the ring assembly to resist the axial rocking of the actuator body relative to the pivot, especially during structural resonance mode [1].

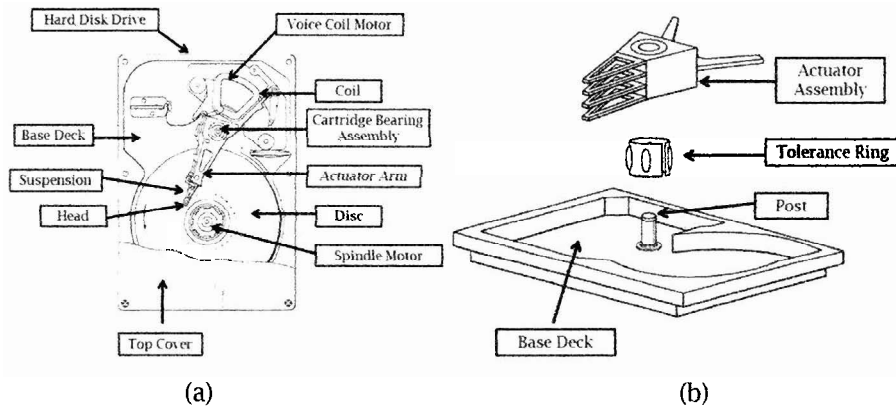


Fig. 1: Hard disk drive. (a) Top plan view, (b) Exploded view.

The tolerance rings are used in HDD for various reasons depending on the design of the tolerance ring, for example, a tolerance ring that provides a low consistent installation force [2] and a tolerance ring which has asymmetric wave [3]. Fig. 2 illustrates a tolerance ring that provides a low consistent installation force. The tolerance ring has a cylindrical body which consists of a number of waves around the cylindrical body. Each wave has a contact surface of an elliptical shape both in the vertical and horizontal axis [2]. As shown in Fig. 3, the tolerance ring has a cylindrical shape with at least two wave rows around the surface of the cylinder. Usually, a tolerance ring has an asymmetric arrangement of the waves to reduce vibration in the actuator arm assembly [3].

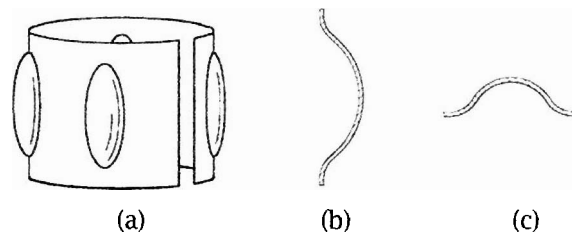


Fig. 2: Tolerance ring. (a) Isometric view, (b) Cross sectional view in a vertical axis and (c) Cross sectional view in a horizontal axis.

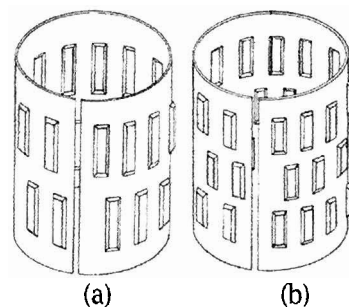


Fig. 3: Tolerance rings. (a) Two wave rows and (b) Three wave rows.

The purpose of the new tolerance ring designs studied in this research is to decrease the installation forces and the total deformations of the tolerance ring whereas the natural frequencies of all pivot butterfly modes remain within the specifications. Ultimately, this can help improving the chance to increase the number of reworking process cycle in the manufacturing and to reduce the costs of the production [5-8]. In this research, we primarily explore two geometric design concepts of the tolerance ring's wave, which are the vertical and horizontal curve designs. Each concept comprises of symmetric and asymmetric arrangement of the waves. In order to compare these designs, the finite element method is employed to perform the static structural and modal analyses. The static structural analysis provides the solutions of the installation forces and total deformations, whereas the modal analysis supports the information of various mode shapes and natural frequencies. In this research, all finite element analyses (FEA) are performed by using ANSYS software.

## 2 MATHEMATICAL MODEL

According to contact surface areas between the tolerance ring waves and the inner surface of the e-block, the tolerance ring in Fig. 4 is equivalent to the mass in Fig. 5(a), the e-block in Fig. 4 is equivalent to the surface in Fig. 5(a), and the tolerance ring waves in Fig. 4 are equivalent to the stiffness (k) in Fig. 5(a).

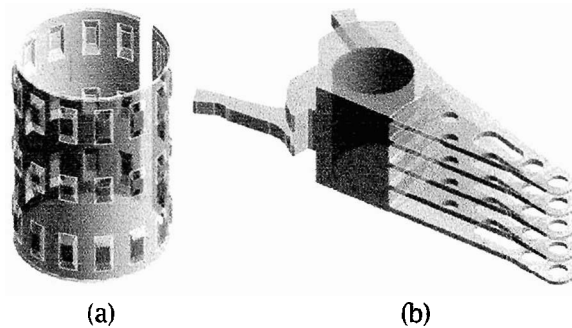


Fig. 4: Contact surface between a tolerance ring and an e-block for current design.  
 (a) Contact surfaces of a tolerance ring and (b) Contact surface of an e-block.

### 2.1 Free Vibration of the One Dimensional Undamped Systems

The general form of the differential equation for free vibration of a one degree of freedom undamped system is shown in equation 2.1. The general solution of differential equation is shown in equation 2.2 [4].

$$m\ddot{x} + kx = 0 \quad (2.1)$$

$$x(t) = x_0 \cos \omega_n t + \frac{\dot{x}_0}{\omega_n} \sin \omega_n t \quad (2.2)$$

$$\omega_n = \sqrt{\frac{k}{m}} \quad (2.3)$$

Where  $\omega_n$  is the natural frequency

## 2.2 Free Vibration of the One Dimensional Systems with Coulomb Damping

### 2.2.1 Damping

Damping is an energy dissipation mechanism that causes vibrations to diminish over time and eventually stop. The amount of damping depends on the material, the velocity of motion and the frequency of vibration. Damping can be classified into 3 groups.

#### 2.2.1.1 Viscous Damping

Viscous damping force is proportional to the velocity of the vibrating body. This type of damping occurs when a body moves through a fluid such as dashpot or shock absorber.

#### 2.2.1.2 Hysteretic Damping

Hysteretic damping is inherently present in the material behavior that energy is dissipated by internal friction. The energy dissipated by internal friction in a real system does not depend on frequency.

#### 2.2.1.3 Coulomb Damping (Dry Friction Damping) [4]

Coulomb damping is the damping that occurs due to dry friction when two surfaces slide against one another. Coulomb damping can be a result of a mass sliding on a dry surface such as the tolerance ring and the e-block or the tolerance ring and the pivot assembly.

The mass of Fig. 5(a) slides on a dry surface, a friction force that resists the motion develops between the mass and the surface. Coulomb's law states that the friction force is proportional to the normal force developed between the mass and the surface. The constant of proportionality  $\mu$ , is called the kinetic coefficient of friction. Since the friction force always resists the motion, its direction depends on the sign of the velocity.

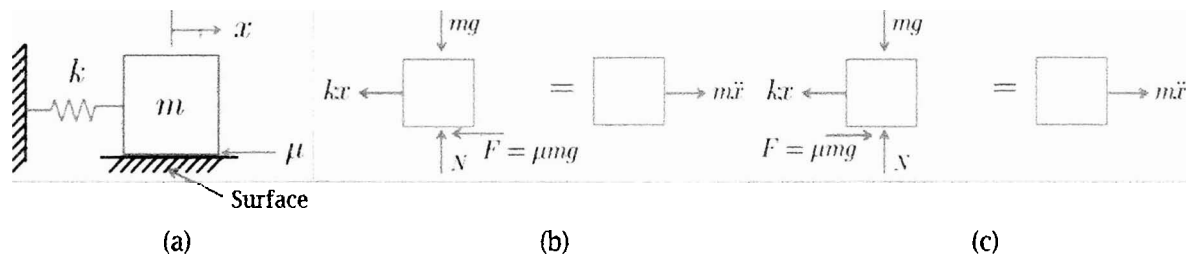


Fig. 5: Free body diagram. (a) Mass slides on a surface with a kinetic coefficient of friction  $\mu$ , (b) Free body diagrams at an arbitrary instant of time when  $\dot{x} > 0$ , and (c) Free body diagrams at an arbitrary instant of time when  $\dot{x} < 0$ .

Application of Newton's law to the free body diagrams of Fig. 5(b) and Fig. 5(c) yields the following differential equations as shown in equation 2.4 and 2.5. Where  $\mu$  is the coefficient of friction,  $m$  is the mass and  $g$  is the gravitational constant.

$$m\ddot{x} + kx = -\mu mg; \dot{x} > 0 \quad (2.4)$$

$$m\ddot{x} + kx = \mu mg; \dot{x} < 0 \quad (2.5)$$

The general form of the differential equation governing the free vibrations of a linear system where Coulomb damping is the only source of damping is equation 2.6 and 2.7. where  $F_f$  is the magnitude of the Coulomb damping force.

$$\ddot{x} + \omega_n^2 x = -\frac{F_f}{\tilde{m}}; \dot{x} > 0 \quad (2.6)$$

$$\ddot{x} + \omega_n^2 x = \frac{F_f}{\tilde{m}}; \dot{x} < 0 \quad (2.7)$$

In this research, we consider the free vibration of the one dimensional undamped system as shown in the equations 2.1 to 2.3, and the free vibration of the one dimensional undamped system with Coulomb damping as shown in the equation from 2.4 to 2.7. Free vibrations are oscillations about a system's equilibrium position that occur in the absence of an external excitation. Free vibrations are result of a kinetic energy imparted to the system or of a displacement from the equilibrium position that leads to a difference in potential energy from the system's equilibrium position.

We design the tolerance rings based on the equations 2.1 to 2.7. The natural frequencies from equation 2.3 depend on the stiffness and the mass. By changing the geometry of the wave from a flat surface to a curved surface, it would affect in a decrease in the mass and increase in the natural frequency as shown in the equations 2.3. Moreover, this change will also lessen the contact surface areas, which will consequently reduce the installation force as shown in the equations 2.4 to 2.7.

### 3 FINITE ELEMENT ANALYSIS

In this research, we examine and compare three important parameters, which are the installation force, the total deformation and the natural frequency. The first two parameters are analyzed by the static structural finite element method. The natural frequency and mode shape are provided by the modal finite element analysis. The goal of the tolerance ring design is to reduce the value of installation forces during APFA assembly process and reduce the total deformations of tolerance ring in order to increase the number cycle of reworking process of the tolerance ring in manufacturing.

#### 3.1 Installation Forces

##### 3.1.1 Components of APFA

An APFA consists of the coil, pivot shaft, two bearings, pivot sleeve, damper, tolerance ring and e-block. For simplicity, in this research, we only consider three important components in the finite element analysis as shown in Fig. 6.

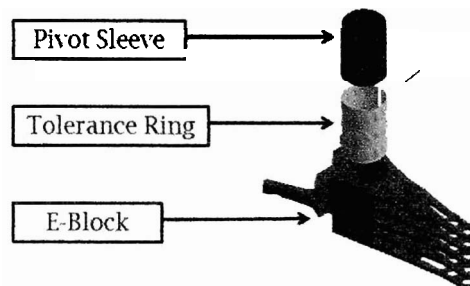


Fig. 6: Assembly process.

##### 3.1.2 Finite element analysis of the installation forces for the current design

Fig. 7(a) illustrates the finite element model using the current design of the tolerance ring. The whole model consists of 107,504 nodes and 53,552 elements, and the tolerance ring has 86,435 nodes and 42,669 elements as shown in Fig. 7(b). The top and bottom surfaces of the e-block are fixed as shown in the blue area of Fig. 7(c). The interaction between the waves of the tolerance ring and the inner surface of the e-block are set under a frictional contact condition.

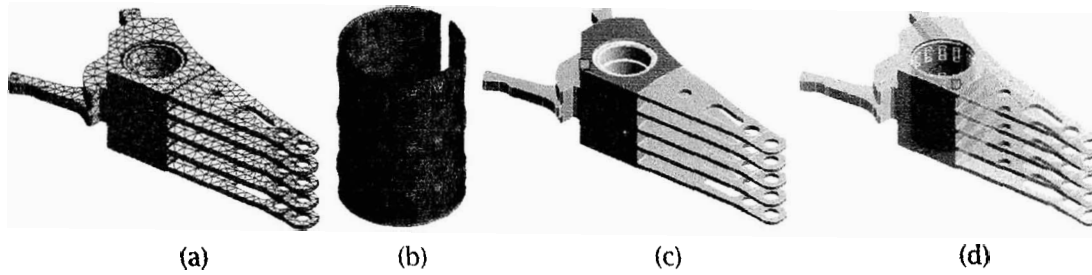


Fig. 7: Finite element model of installation forces. (a) Meshing, (b) Meshing of the tolerance ring, (c) The areas of the fixed constraint and (d) Frictional contact surfaces between the tolerance ring and the e-block.

Fig. 8 illustrates the simulation steps of the tolerance ring installation process. This process is analyzed using the static structural method, and the resulting installation forces can be measured from the reaction forces occurred at contact surfaces between the tolerance ring and the e-block as shown in Fig. 9.

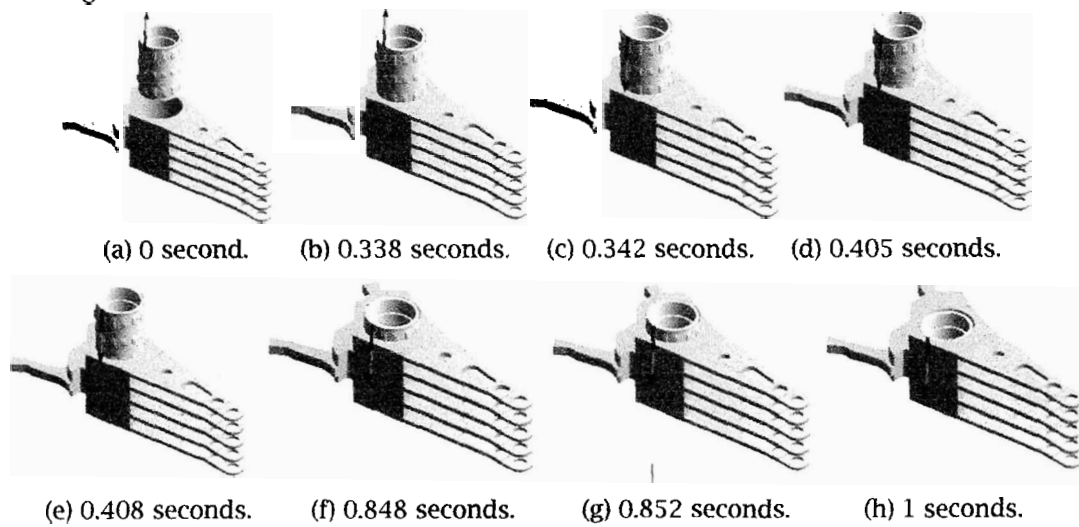


Fig. 8: Finite element simulation of the installation process.

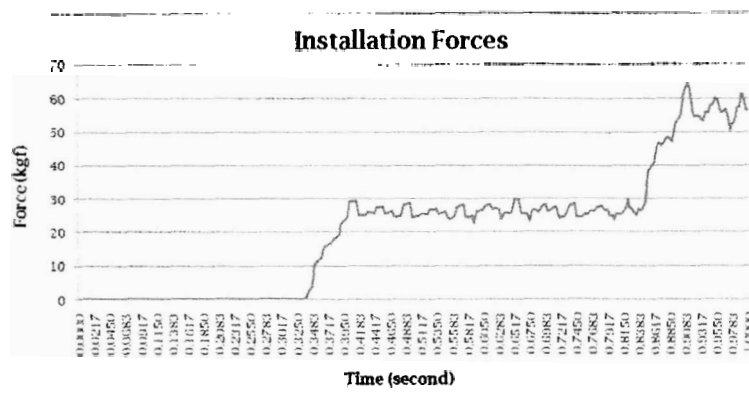


Fig. 9: Installation forces graph for current design.

According to the results shown on Fig. 9 in overall, there is a considerable increase in the value of the installation force during 1 second. During the first 0.338 seconds, the installation force value is approximately 0.0589 kilogram forces, but this force rises rapidly in the next 0.063 second (0.342-0.405 seconds). This increase is due to the friction between the wave in the bottom row and the inner surface of the e-block. In the following 0.440 seconds (0.408-0.848 seconds), the installation force value remains at approximately 24.4 kilogram forces. This is because the height of the waves in the middle is less than those in the top and bottom rows for approximately 10 microns. Therefore, the waves in the middle row are not in contact with the inner surface of the e-block. After that, the forces grow significantly from 26.843 kilogram forces to 52.485 kilogram forces. This increase is due to friction between the waves in the top row and the e-block. The installation forces reach a peak of 59.697 kilogram forces in 0.912 seconds.

### 3.2 Total Deformations

The values of total deformations can be calculated using equation 2.8.

$$U = \sqrt{U_x^2 + U_y^2 + U_z^2} \quad (2.8)$$

$U$  = Total deformation,  $U_x$  = Deformation in X-axis,  $U_y$  = Deformation in Y-axis, and

$U_z$  = Deformation in Z-axis.

#### 3.2.1 Finite element analysis of total deformations for the current design

The same structural analysis used to analyze the installation force is used to analyze the total deformation. Fig. 10(a) shows the deformation results from the simulation. The maximum value of the total deformation is approximately 5.4179 microns, which occurs at the peaks of all waves in the top and bottom row.

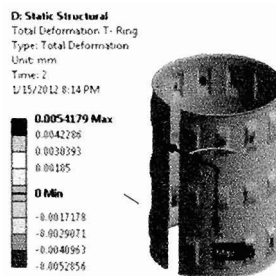


Fig. 10: The resulting total deformation

### 3.3 Natural Frequencies

The natural frequency and the mode shape of the APFA are analyzed using the finite element modal analysis. Results show that the mechanical vibration of APFA has various mode shapes such as coil bending, coil torsion, 1<sup>st</sup> pivot butterfly, arm torsion, arm scissor, 2<sup>nd</sup> pivot butterfly and 3<sup>rd</sup> pivot butterfly as shown in Fig. 11(a) - 11(f), where each mode shape has different natural frequency.



(a) Coil Bending.

(b) Coil Torsion.

(c) 1<sup>st</sup> Pivot Butterfly.



(d) Arm Torsion. (e) 2<sup>nd</sup> Pivot Butterfly. (f) 3<sup>rd</sup> Pivot Butterfly.

Fig. 11: Mode shapes. (a) Coil Bending, (b) Coil Torsion, (c) 1<sup>st</sup> Pivot Butterfly, (d) Arm Torsion, (e) 2<sup>nd</sup> Pivot Butterfly and (f) 3<sup>rd</sup> Pivot Butterfly.

### 3.3.1 Finite element analysis of natural frequencies for the current design

Fig. 12(a) illustrates the finite element model of APFA with 318,095 nodes and 153,552 elements. The top and bottom surfaces of the pivot shaft are fixed as shown as the blue circle in Fig. 12(b). All contact surfaces are bonded, which means that there is no sliding or separation between surfaces.

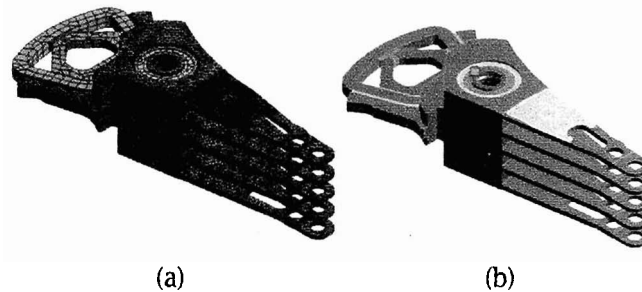


Fig. 12: Finite element model of APFA. (a) Meshing and (b) Area with fixed constraint.

The natural frequency obtained from the finite element analysis is compared with the data measured by LDV (Laser Dropper Vibrometer) and the specification for validation.

In this research, the validation of finite element analysis will be considered for 1<sup>st</sup> Pivot Butterfly, 2<sup>nd</sup> Pivot Butterfly and 3<sup>rd</sup> Pivot Butterfly mode because the exact specifications are available for these modes. Tab. 1 shows the percentage errors of the finite element results comparing to the specification and the values measured by LDV for the first, second and third pivot butterfly modes. The percentage error when comparing to the LDV data are 6.63, 0.25 and 0.13 respectively, and the percentage error when comparing to the specification are 0.85, 0.35 and 0.16 respectively. The low percentage error indicates the reliability of finite element model. Therefore, this finite element model is validated.

Mode Shape	Natural Frequency (Hz)			The Percentage Errors (LDV)	The Percentage Errors (Spec)
	LDV	Spec.	FEA		
1 <sup>st</sup> Pivot Butterfly	6740	6240	6293.2	6.63	0.85
2 <sup>nd</sup> Pivot Butterfly	11800	11870	11829	0.25	0.35
3 <sup>rd</sup> Pivot Butterfly	17560	17610	17582	0.13	0.16

Tab. 1: Comparison natural frequencies between FEA and Specification.

## 4 THE TOLERANCE RING DESIGN CONCEPT

### 4.1 The current design

The current design of the tolerance ring consists of three wave rows. Looking at the vertical and horizontal cross sections, the geometries of three wave rows are the flat surfaces as shown in Fig. 13(b) and 13(c). The contact areas between two surfaces are the square areas on the top and bottom rows as shown in Fig. 13(a).

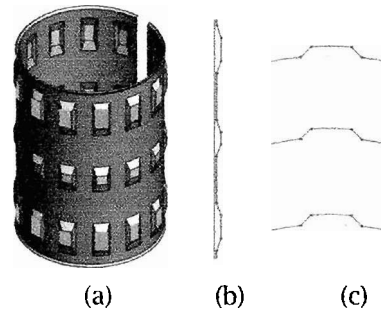


Fig. 13: Current design. (a) Isometric view,  
(b) Cross section in the vertical axis and (c) Cross section in the horizontal axis.

### 4.2 The vertical curve design

The first design is the vertical curve design as shown in Fig. 14(a). The concept of this design is to decrease the contact surface area between the waves of the tolerance ring and the inner surface of the e-block by adapting the wave geometry from a flat surface to a curved surface. The first design is to smooth the surface in the vertical direction as shown in Fig. 14(b). Since the curved surface provides less contact area with respect to the present design, therefore the installation force between both surfaces is reduced during APFA assembly process when comparing to the current design. However, this might affect in more vibrations in the actuator arm because of the lower ability to resist the axial rocking motion.

For the vertical curve design, the geometry of the waves in the middle row remains unchanged. Looking at the vertical cross section, the waves are reshaped from flat to curved surfaces. The contact areas between two surfaces become horizontal lines along the top and bottom rows as shown in Fig. 14(a). Looking at the horizontal cross section, the three wave rows remain flat surfaces as shown in Fig. 14(c).

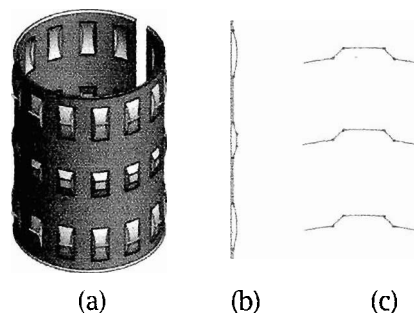


Fig. 14: The vertical curve design. (a) Isometric view,  
(b) Cross section in the vertical axis and (c) Cross section in the horizontal axis.

### 4.3 The asymmetric vertical curve design

The second design is the asymmetric vertical curve design as shown in Fig. 15(a). The concept of this design is to decrease the contact surface areas between the waves of the tolerance ring and the inner surface of the e-block by changing the wave geometry from a flat surface to a curved surface in the vertical direction as shown in Fig. 15(b) and to modify configuration of the waves in the middle row from the symmetric to the asymmetric waves in order to reduce vibration for a pivot bearing in the actuator arm. This asymmetric vertical curve design provides lower vibration problem in the actuator arm, because it is likely to distribute forces at the contact surfaces so that each contact surface receives a lower contact force [3]. As the result, the natural frequencies of vibration in the actuator arm are decreased.

For the asymmetric vertical curve design, the geometry of the waves in the middle row remains unchanged, but the arrangements of the waves become asymmetric. The contact areas between two surfaces become horizontal lines along the top and bottom rows as shown in Fig. 15(a). Looking at the horizontal cross section, the three wave rows remain flat surfaces as shown in Fig. 15(c).

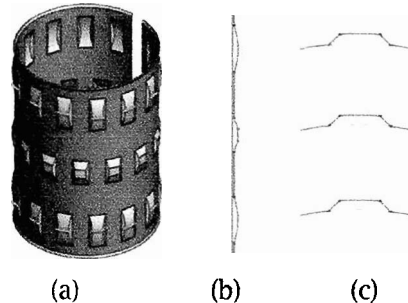


Fig. 15: The asymmetric vertical curve design. (a) Isometric view, (b) Cross section in the vertical axis and (c) Cross section in the horizontal axis.

### 4.4 The horizontal curve design

The third design is the horizontal curve design as shown in Fig. 16(a). The concept of this design is to decrease the contact surface area by adapting the wave geometry from a flat surface to a curved surface in the horizontal direction as shown in Fig. 16(c). The curved surface provides less contact area with respect to the present design. Therefore, the installation force between both surfaces is reduced during APFA assembly process when comparing to the current design. However, this might affect in more vibrations in the actuator arm because of the lower ability to resist the axial rocking motion.

For the horizontal curve design, the geometry of the waves in the middle row remains unchanged. Looking at the horizontal cross section, the waves are reshaped from flat to curved surfaces. The contact areas between two surfaces become vertical lines along the top and bottom rows as shown in Fig. 16(a). Looking at the vertical cross section, the three wave rows remain flat surfaces as shown in Fig. 16(b).

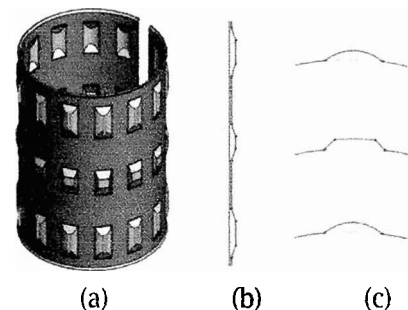


Fig. 16: The horizontal curve design. (a) Isometric view, (b) Cross sectional view in the vertical axis and (c) Cross sectional view in the horizontal axis.

#### 4.5 The asymmetric horizontal curve design

The fourth design is the asymmetric horizontal curve design as shown in Fig. 17(a). The concept of this design is to decrease the contact surface area between the waves and the inner surface of the e-block by changing the wave geometry from a flat surface to a curved surface in the horizontal direction as shown in Fig. 17(c) and to modify configuration of the waves in the middle row from the symmetric to the asymmetric waves in order to reduce vibration for a pivot bearing in the actuator arm. This asymmetric horizontal curve design provides lower vibration problem in the actuator arm, because it is likely to distribute forces at the contact surfaces so that each contact surface receives a lower contact force [3]. As the result, the natural frequencies in the actuator arm are decreased.

For the asymmetric horizontal curve design, the geometry of the waves in the middle row remains unchanged, but the arrangements of the waves become asymmetric. The contact areas between two surfaces become vertical lines along the top and bottom rows as shown in Fig. 17(a). Looking at the vertical cross section, the three wave rows remain flat surfaces as shown in Fig. 17(b).

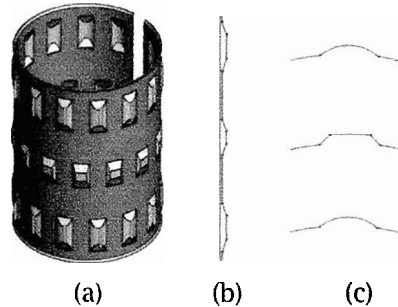


Fig. 17: The asymmetric horizontal curve design. (a) Isometric view, (b) Cross section in the vertical axis and (c) Cross section in the horizontal axis.

#### 4.6 The alternating flat-curve design

The fifth design is the alternating flat-curve design as shown in Fig. 18(a). According to the first four designs, we found that the natural frequency of the third pivot butterfly mode is close to the upper boundary of the specification and the installation forces are close to the lower boundary of the specification. Therefore, the concept of this design is to increase some contact surface areas between the waves and the e-block by alternating of the wave geometry between flat and curved surface. As the result, the increase of the contact surface areas causes less vibrations in the actuator arm and higher the installation forces.

For the alternating flat-curve design, the geometry of the waves in the middle row remains unchanged, but the arrangements of the waves become asymmetric. The waves in the top and bottom rows have alternately reconfigured from the flat to the curved surface as shown in Fig. 18(c). The contact areas between two surfaces become vertical lines and square areas along the top and bottom rows as shown in Fig. 18(a). Looking at the vertical cross section, the three wave rows remain flat surfaces as shown in Fig. 18(b).

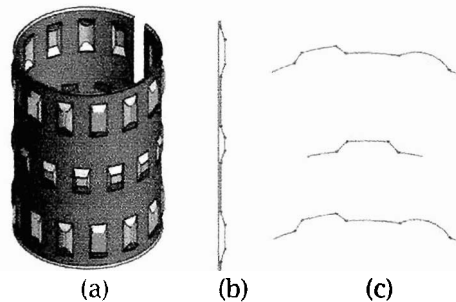


Fig. 18: The alternating flat-curve design. (a) Isometric view, (b) Cross section in the vertical axis and (c) Cross section in the horizontal axis.

## 5 EXPERIMENTAL RESULTS

We compare the results among the five designs by considering three important parameters which are the installation forces, the total deformations and the natural frequencies.

### 5.1 Installation Forces

The plot in Fig. 19 compares the installation force results of the current design and those of the five new designs. The specification of the installation force should be within 15 to 120 kilogram forces. According to the results, the values of the installation force of the new five designs are less than the current design, since contact surface areas is reduced. The installation force of vertical curve design and the asymmetric vertical curve design are 13.49 and 13.48 kilogram forces, respectively, which are lower than the range of specification. Whereas the values of the installation force of the horizontal curve design, the asymmetric horizontal curve and the alternating flat-curve design remain within the specification. According to the comparison in Fig. 19, the alternating flat-curve gives the best installation force result among all, since the installation force value is closer to the mid value of the specifications range than the horizontal curve and the asymmetric horizontal curve design.

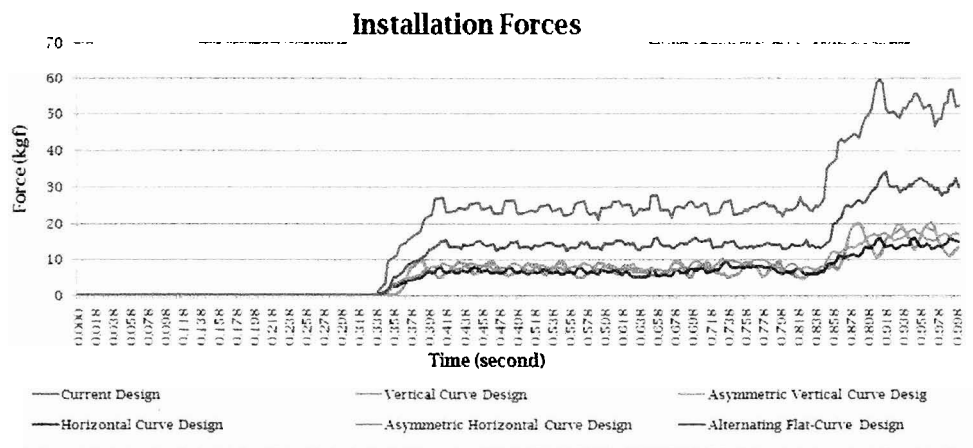


Fig. 19: Installations forces of all designs.

### 5.2 Total Deformations

Fig. 20. shows the comparison of the total deformation results of the current design and those the five new design. According to the result, the total deformation of the vertical curve design and the asymmetric vertical curve design are more than that of the current design for approximately 1.43 and 2.30 microns, respectively. This is because the contact surfaces of both designs are perpendicular to the direction for the assembly process. Whereas the values of the total deformation of the horizontal curve design and the asymmetric horizontal curve design are less than the current design for approximately 1.5 and 0.93 microns, because the contact surface of both designs are parallel to the direction of installation process. Therefore, the horizontal curve design and the asymmetric horizontal curve design are the good solutions to decrease the total deformation value.

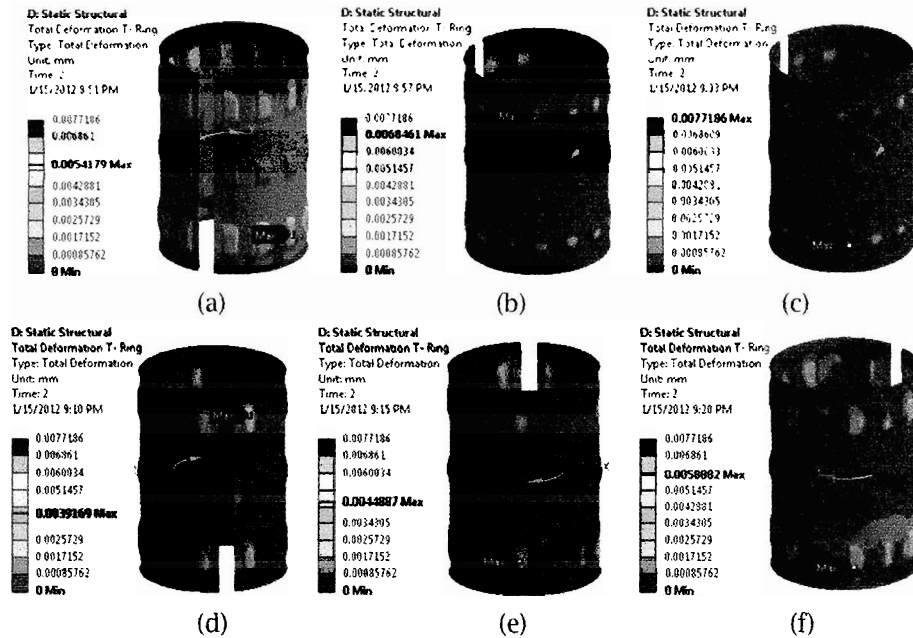


Fig. 20: Total deformations of all designs. (a) The current design, (b) The vertical curve design, (c) The asymmetric vertical curve design, (d) The horizontal curve design, (e) The asymmetric horizontal curve design and (f) The alternating flat-curve design.

### 5.3 Natural Frequencies

The Tab. 2 shows that the natural frequency values of all the new designs are higher than that of the current design, because all new designs reduce the contact surface areas between the waves and the e-block, and have lower resistance to the axial rocking motion. The natural frequency values for the third butterfly mode of the vertical curve design and the asymmetric vertical curve design illustrate 18,211 and 18,202 hertz, respectively. The natural frequency values of these two new designs are more than the upper boundary of the specification. Whereas, the natural frequency values of the horizontal curve design and the asymmetric horizontal curve design are close to the upper boundary of the specification. However, the alternating flat-curve design can decrease the natural frequency value of the third pivot butterfly mode to a value closer to the mid value of the specification.

Mode Shape	Current Design	Vertical Curve	Asymmetric Vertical Curve	Horizontal Curve	Asymmetric Horizontal Curve	Alternating Flat-Curve
Coil Bending	2424.8	2428.3	2428.7	2428.3	2428.1	2426.2
Coil Torsion	4523.3	4533.0	4533.1	4530.7	4530.1	4526.7
1 <sup>st</sup> Pivot Butterfly (5650-6840)	6293.2	6488.6	6488.4	6431.6	6416.4	6351.1
Arm Torsion	7650.2	7719.2	7718.3	7692.2	7684.4	7665.7
2 <sup>nd</sup> Pivot Butterfly (11610-12140)	11829	11860	11860	11850	11847	11835
3 <sup>rd</sup> Pivot Butterfly (17170-18050)	17582	18211	18202	18029	17974	17726

Tab. 2: Comparison of the natural frequencies (Hz).

## 6 CONCLUSION

The installation force values of all the new designs are less than the current design since the contact surface areas are decreased. The total deformation values of the horizontal curve design and the asymmetric horizontal curve design are lower than the current design, whereas the natural frequency values of the third pivot butterfly mode of these two designs are close to the upper boundary of the specification. However, the natural frequency of the alternating flat-curve design is still within the specification and close to the mid value of the specification. Therefore, the horizontal curve design, the asymmetric horizontal curve design and the alternating flat-curve design are the best three solutions for the new concept designs to reduce the installation force and the total deformation.

This study of the tolerance ring's new design concept benefits the future possibility to increase the number of reworking process cycle of the tolerance ring in the HDD manufacturing process. The increasing number of the reworking process of the tolerance ring can help increasing the productivity and efficiency in the HDD manufacturing. For the future work, the effect of the three design variables, which are the height, width and amount of waves of the tolerance ring, will be considered and analyzed together in order to conclude the optimized tolerance ring design.

## ACKNOWLEDGEMENTS

This research is financially supported by the National Electronics and Computer Technology Center (NECTEC), Industry/University Cooperative Research Center in HDD Advanced Manufacturing, King Mongkut's University of Technology Thonburi, and receives information from Western Digital (Thailand) Co., Ltd.

## REFERENCES

- [1] Walter, L. P.: Hard Disk Drive Actuator Assembly with Damped Tolerance Ring for Enhancing Drive Performance during Structural Resonance Modes, United States Patent, 6,480,363 B1, Nov. 12, 2002.
- [2] Nigel, F. M.; Denis, A. S.; Inman, L. J.: Tolerance Ring with Low Consistent Installation Force Profile, United States Patent, 6,333,839 B1, Dec. 25, 2001.
- [3] Kevin, P. H.; Ryan, J. S.; David, D. D.: Tolerance Ring Having Variable Height and/or Asymmetrically Located Bumps, United States Patent, 7,580,225 B2, Aug. 25, 2009.
- [4] S. Graham Kelly: Fundamentals of Mechanical Vibrations, Second Edition, McGraw-Hill, 2000.
- [5] Somkid, S.; Arbtip, D.: Finite Element Analysis of a Reworking Process of a Tolerance Ring in a HDD's Actuator Arm, DST-CON 2011 The 4th International Data Storage Technology Conference, 2011.
- [6] Kamran, O.; Chen, C. L.: Disk Drive Including Pivot-Bearing Cartridge Tolerance Ring Having a Damping Layer for Actuator Resonance Reduction, United States Patent, 7,085,108 B1, Aug. 1, 2006.
- [7] Kevin, P. H.; David, D. D.; Ryan, J. S.; Matthew, S. S.: Tolerance Ring with High Axial Static Friction, United States Patent, 7,611,303 B2, Nov. 3, 2009.
- [8] Daryl, L. L.: A First Course in The Finite Element Method, Fourth Edition, Thomson Press, University of Wisconsin-Platteville, Canada, 2007.